Derivation of Hawking radiation in dispersive dielectric media

Malte F. Linder and Ralf Schützhold*
Fakultät für Physik, Universität Duisburg-Essen, Lotharstraße 1, 47057 Duisburg, Germany

William G. Unruh†
Department of Physics and Astronomy, University of British Columbia, Vancouver, British Columbia V6T 1Z1, Canada
(Dated: May 6, 2016)

Motivated by recent experimental efforts, we study a black hole analog induced by the propagation of a strong laser pulse in a nonlinear dielectric medium. Based on the Hopfield model (one pair of Sellmeier coefficients), we perform an analytic and fully relativistic microscopic derivation of the analog of Hawking radiation in this setup. The Hawking temperature is determined by the analog of the surface gravity (as expected), but we also find a frequency-dependent gray-body factor (i.e., a nonthermal spectrum at infinity) due to the breaking of conformal invariance in this setup.

PACS numbers: 04.70.Dy, 04.62.+v, 04.80.-y, 42.50.-p

arXiv:1511.03900v2 [gr-qc] 6 May 2016

I. INTRODUCTION

Hawking's prediction [1, 2] that black holes evaporate due to quantum effects has been one of the most striking consequences of quantum field theory in curved spacetimes and is also expected to have profound implications for the theory of quantum gravity. Unfortunately, however, our chances for observing this phenomenon are very feeble since small enough black holes for their radiation to be observable probably do not exist. Nevertheless, according to the suggestion [3] by one of the authors, it might be possible to recreate this fundamental quantum effect in the laboratory via suitable analogs. The original proposal was based on the propagation of sound in fluids which can generate sonic or acoustic analogs of black holes (also known as dumb holes). The microscopic derivation of the sonic analog of Hawking radiation (including changes in the dispersion relation at small wavelengths) has been studied by many authors and is now quite well understood; see, e.g., Refs. [4–19]. Recently, there has been remarkable experimental progress regarding the efforts to observe signatures of the Hawking effect in Bose–Einstein condensates [20–24]. For the sake of completeness, we would also like to mention other scenarios (see, e.g., Refs. [25–34]) such as water waves [31], where the classical analog of the Hawking effect has been observed recently [35, 36].

However, apart from the sonic analogs, there is also another very interesting option—optical or dielectric black hole analogs or, more generally, electromagnetic setups [37–48]. In these scenarios, the fluid flow is typically replaced by the motion of an optical or electromagnetic pulse through the material. Even though there have been several interesting experimental efforts [49–54] along this line, our theoretical understanding (e.g., regarding the impact of dispersion) is far less advanced than in the case of the sonic analogs [4–19]. Apart from numerical simulations (see, e.g., Refs. [42, 44]), only a very few analytical results (in analogy to the sonic case) are available. For example, Ref. [47] presents a derivation based on an approximation where one output channel is neglected. However, as we shall see below, this approximation is in general not fully justified and gives incorrect results. As another example, the horizon is replaced by a step-function profile in Refs. [43, 46]. For this simplified setup, the spectrum can also be calculated analytically. However, because the step function formally corresponds to an infinite surface gravity, questions such as the thermality of the spectrum and the relation between the analog Hawking temperature and the surface gravity cannot be addressed in this simplified setup. Here, we contribute to filling this gap (see also Refs. [43, 45–47, 55]) and provide a microscopic derivation of the analog of Hawking radiation based on a minimal set of assumptions/approximations.

II. THE MODEL

In order to describe Hawking radiation induced by a strong, classical light pulse in a homogeneous and transparent dielectric medium, we employ the following microscopic model, suggested in Ref. [37] and further developed in Refs. [43, 45–47]. This model is closely inspired by the Hopfield model [56, 57]. For simplicity, we assume spatial symmetry of the medium and of the pulse along the y and z axes (plane symmetry). We also restrict ourselves to one fixed polarization of the pulse $\boldsymbol{E}_{\rm pulse} \propto \boldsymbol{e}_y$ [(1+1)-dimensional model]. Additional low-intensity light "on top" of the pulse (e.g., Hawking radiation and other quantum perturbations) with the same polarization can thus be described by the vector potential $\boldsymbol{A}(t,x) = A(t,x)\boldsymbol{e}_y$ via $\boldsymbol{E}_{\rm weak} = \partial_t \boldsymbol{A}$ in temporal gauge. This weak electromagnetic field will interact with the strong pulse via the medium's polarizable charges, which are already excited beyond the linear range due to the (local) intensity of the strong pulse. The weak field

* ralf.schuetzhold@uni-due.de
† unruh@physics.ubc.ca

will cause additional deformations of the excited states; however, we assume that these deformations are within the linear regime around the polarized states influenced by the pulse alone. Hence, each polarizable charge is assumed to interact like a scalar (one polarization) harmonic oscillator with the weak field. We restrict the weak field to large wavelengths compared to the molecular scale of the dielectric (e.g., Hawking radiation with a low temperature), so we can consider the dielectric in the continuum limit and not worry about the dispersion changes created due to the finite distances between the polarizable molecules of the medium.

This model is as follows: there is one harmonic oscillator at each point in space, the electric dipole displacement being described by the scalar field $\psi(t,x)$. The eigenfrequency $\Omega > 0$ of a specific oscillator depends on the local classical pulse intensity, so $\Omega = \Omega(t,x)$. This change in the local frequency of the dipoles is assumed to be the only effect of the strong pulse in our model. In terms of the atoms/molecules constituting the nonlinear medium, this local frequency models the level spacing and hence its change can be understood in terms of the quadratic Stark shift $\Omega(t,x) \approx \Omega_0 - \alpha_{\text{Stark}} \boldsymbol{E}^2_{\text{strong}}(t,x)$. Note that the strong pulse could in principle also modify the dipole matrix elements which determine the coupling between the atoms and the weak field—but we shall largely omit this effect in our model.

Neglecting any backreaction of the weak fields A and ψ on the strong pulse or the frequency changes in Ω or coupling g that the strong pulse induces, the dynamics of A and ψ are thus described by the Lagrangian density ($c_0 = \varepsilon_0 = \mu_0 = \hbar = k_B = 1$)

$$\mathcal{L}_{\text{lab}} = \overbrace{\frac{1}{2}\left(|\partial_t A|^2 - |\partial_x A|^2\right)}^{\text{weak EM field}} + \overbrace{\frac{1}{2}\left(|\partial_t \psi|^2 - \Omega^2 |\psi|^2\right)}^{\text{medium (oscillators)}} + \underbrace{g\,\text{Re}(\psi \partial_t A^*)}_{\text{interaction}} \tag{1}$$

in the laboratory frame (rest frame of the dielectric medium). The Lagrangian density consists of the contributions from the free weak electromagnetic field $(\boldsymbol{E}^2_{\text{weak}} - \boldsymbol{B}^2_{\text{weak}})/2$, the harmonic oscillators, and the interaction between the polarization perturbation ψ and the electric field $\boldsymbol{E}_{\text{weak}} = \partial_t A \boldsymbol{e}_y$. The nonlinear optical influence of the strong pulse on the dielectric is encoded in the space-time–dependent eigenfrequency $\Omega(t,x)$ and potentially the coupling constant $g(t,x) > 0$, which we assume in the following are both prescribed fields. It is advantageous for the following analysis to generalize A and ψ to complex scalar fields, so $\mathcal{L}_{\text{lab}}$ has been defined accordingly.

A. Speed of light in static medium

Let us begin by deriving the well-known Sellmeier dispersion relation from the model (1) in a static medium. This will show us how to describe a dispersive dielectric—which then includes the possibility of inducing analog black hole event horizons for light via the strong light pulse (see also Refs. [43, 46, 47]). By means of Hamilton's principle, $\mathcal{L}_{\text{lab}}$ yields the equations of motion

$$(\partial_t^2 - \partial_x^2) A = -\partial_t (g\psi) \,, \tag{2a}$$

$$(\partial_t^2 + \Omega^2)\psi = g \partial_t A \,. \tag{2b}$$

In order to gain a rough insight into the physics of the model, we assume a static medium $\partial_t \Omega = \partial_t g = 0$ for the moment. Then, there are stationary solutions, each with a unique frequency ω_{lab}. For these solutions, we can substitute $\partial_t^2 \psi \to -\omega_{\text{lab}}^2 \psi$ and $\partial_t^2 A \to -\omega_{\text{lab}}^2 A$ in the above equations. Then, solving Eq. (2b) for ψ and inserting the result back into Eq. (2a) leads to

$$\left(-\frac{\omega_{\text{lab}}^2}{c_{\text{lab}}^2} - \partial_x^2\right) A = \left(\frac{1}{c_{\text{lab}}^2}\partial_t^2 - \partial_x^2\right) A = 0 \tag{3}$$

with the frequency-dependent (phase) velocity of light

$$c_{\text{lab}}(\omega_{\text{lab}}) = \left(1 + \frac{g^2}{\Omega^2 - \omega_{\text{lab}}^2}\right)^{-1/2} . \tag{4}$$

Note that we obtain the dispersion relation with only one pole at $\omega_{\text{lab}} = \Omega$ and one Sellmeier coefficient g because we considered just one polarization field, ψ. Multiple medium resonances were considered in Refs. [43, 45–47]. This was motivated by the experiments [49, 50] in fused silica. Here, we assume that the material (e.g., diamond, cf. Refs. [43, 44, 58]) is well approximated by one Sellmeier pole.

The model exhibits subluminal dispersion since c_{lab} decreases for increasing ω_{lab}. At $\omega_{\text{lab}} = \Omega$ (resonance frequency of the medium), the speed of light formally drops to zero, which marks the breakdown of the model. We will consequently restrict ourselves to lower frequencies $|\omega_{\text{lab}}| < \Omega$ (e.g., sufficiently low Hawking temperatures) in the remainder of this paper. For very low frequencies, the velocity of light becomes

$$c_{\text{low}} = c_{\text{lab}}(\omega_{\text{lab}} = 0) = \left(1 + \frac{g^2}{\Omega^2}\right)^{-1/2} . \tag{5}$$

For slowly space-time–dependent Ω and g, the result (4) can still be approximately valid provided that A and ψ oscillate very fast compared to the scales on which Ω and g vary [Jeffreys–Wentzel–Kramers–Brillouin (JWKB) approximation]. Within this approximation, the strong pulse can give rise to a space-time–dependent speed of light profile $c_{\text{low}}(t,x)$ in the dielectric medium. However, we cannot use this JWKB approximation throughout because Hawking radiation (or, more generally, particle creation) is precisely associated with a breakdown of this JWKB approximation—at least in terms of the usual coordinates t and x; see also Ref. [59]. Therefore, we have to solve the exact wave equation including the full dispersion relation (without neglecting any ω contributions).

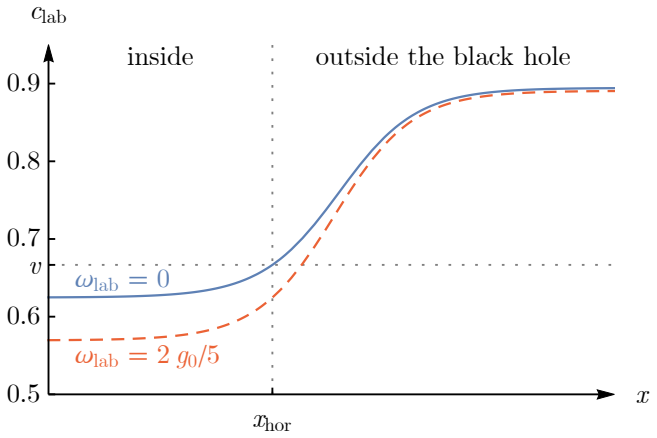

FIG. 1: Plot of a spatial example profile of the speed of light $c_{\rm lab}$ from Eq. (4) in the dielectric, which involves a black hole event horizon analog. In this example, the pulse velocity is $v = 2/3$, the coupling constant $g(t,x) = g_0$ is fixed, and the medium eigenfrequency $\Omega(t,x)$ rises from $4g_0/5$ on the left (smaller values of x) to $2g_0$ on the right with a tanh profile. The plot shows the resulting spatial $c_{\rm lab}$ curves for two different light frequencies. The fastest light waves occur in the low-frequency limit (solid line), so the event horizon is located at the position $x_{\rm hor}$ where these waves propagate at the same speed as the pulse. Light waves with higher frequencies propagate slower (subluminal dispersion) as indicated by the dashed line.

B. Black holes induced by uniformly moving pulses

We focus on strong pulses which travel through the dielectric in the positive x direction with a constant velocity $v \in (0,1)$ and maintain their shapes during the propagation. The external fields Ω and g thus only depend on the quantity $x - vt$. In this setting, the rest frame of the pulse (pulse frame) is a second preferred frame of reference. Its coordinates τ and χ are connected to the laboratory frame coordinates via the Lorentz boost

$$\begin{pmatrix}\tau\\ \chi\end{pmatrix} = \gamma \begin{pmatrix}1 & -v\\ -v & 1\end{pmatrix}\begin{pmatrix}t\\ x\end{pmatrix} \tag{6}$$

with the Lorentz factor $\gamma = 1/\sqrt{1-v^2}$. By assumption, Ω and g are independent of τ in the pulse frame, i.e., $\partial_\tau \Omega = \partial_\tau g = 0$.

A uniformly moving pulse can give rise to an analog of a black hole event horizon in the dielectric; see, e.g., Refs. [38–40, 43, 45–47]. Considered from the laboratory point of view (moving horizon), this will happen if the pulse has such a large intensity at its center that the weak light field propagates slower than the pulse there ($c_{\rm low} < v$), while $c_{\rm low}$ exceeds v outside the inner pulse region (see Fig. 1 for an example pulse profile). Since the dispersion is subluminal—that is, light waves with low frequencies travel at the fastest speed—the event horizon is located at the position where the speed of light for $\omega_{\rm lab} \to 0$ equals the pulse speed,

$$c_{\rm low} = v \quad \Leftrightarrow \quad \Omega = v\gamma g\ . \tag{7}$$

A realistic pulse profile may include multiple horizons fulfilling the condition (7), which could be white as well as black hole horizons. In this paper, however, we will concentrate on a single black hole analog event horizon and aim to calculate the corresponding Hawking spectrum.

III. ANALYSIS IN THE PULSE FRAME

The pulse frame is the most advantageous frame of reference for the derivation of the Hawking effect since the pulse and all associated event horizons are stationary with respect to that frame. The Lagrangian density $\mathcal{L}_{\rm lab}$ in Eq. (1) transformed to the pulse frame reads

$$\begin{aligned}\mathcal{L}_{\rm pls} = {}& \frac{1}{2}\left(|\partial_\tau A|^2 - |\partial_\chi A|^2\right)\\ & + \frac{1}{2}\left[\gamma^2|(\partial_\tau - v\partial_\chi)\psi|^2 - \Omega^2|\psi|^2\right]\\ & + \gamma g\,\mathrm{Re}[\psi(\partial_\tau - v\partial_\chi)A^*]\ .\end{aligned} \tag{8}$$

In this section, we will combine the two equations of motion for A and ψ into a single equality and derive two important and well-known conservation laws from the symmetries of $\mathcal{L}_{\rm pls}$.

A. Stationary modes

The time invariance of $\mathcal{L}_{\rm pls}$ due to $\partial_\tau\Omega = \partial_\tau g = 0$ implies the conservation of the frequency (energy) of any solution (A,ψ) of the equations of motion. Hence, we may concentrate on solutions of the form

$$A(\tau,\chi) = A_\omega(\chi)\mathrm{e}^{-\mathrm{i}\omega\tau}\ , \quad \psi(\tau,\chi) = \psi_\omega(\chi)\mathrm{e}^{-\mathrm{i}\omega\tau} \tag{9}$$

with a unique, conserved pulse frame frequency ω (stationary modes). Inserting this form into the equations of motion (2a) and (2b) transformed to the pulse frame (with $\partial_\tau \to -\mathrm{i}\omega$) leads to the mode equations

$$-(\omega^2 + \partial_\chi^2)A_\omega = \gamma\,(\mathrm{i}\omega + v\partial_\chi)g\psi_\omega\ , \tag{10a}$$

$$\left[\gamma^2(\mathrm{i}\omega + v\partial_\chi)^2 + \Omega^2\right]\psi_\omega = -\gamma g\,(\mathrm{i}\omega + v\partial_\chi)A_\omega\ , \tag{10b}$$

which are satisfied by the mode functions A_ω and ψ_ω.

The mode equations (10a) and (10b) can be combined into one single ordinary differential equation. To this end, we apply the operator $\gamma\,(\mathrm{i}\omega + v\partial_\chi)$, which commutes with $\omega^2 + \partial_\chi^2$, to the upper equation (10a) and then insert Eq. (10b) divided by g. This results in the decoupled fourth-order mode equation

$$\begin{aligned}\Big\{(\omega^2 + \partial_\chi^2)\frac{1}{g}\left[\gamma^2(\mathrm{i}\omega + v\partial_\chi)^2 + \Omega^2\right]\\ - \gamma^2(\mathrm{i}\omega + v\partial_\chi)^2 g\Big\}\psi_\omega = 0\end{aligned} \tag{11}$$

for the mode function ψ_ω. It is important to note that a difference between this equation and the usual equations used in much of the analog model literature is that this is not a second order equation in time. In order to calculate the corresponding function A_ω, which is uniquely determined by a given solution ψ_ω of Eq. (11), we apply the operator $(\mathrm{i}\omega - v\partial_\chi)$ on Eq. (10b) and use this result to eliminate the term $\partial_\chi^2 A_\omega$ in Eq. (10a), which gives

$$A_\omega = \frac{\gamma^2}{\omega^2}\left\{(\mathrm{i}\omega - v\partial_\chi)\frac{1}{\gamma g}\left[\gamma^2(\mathrm{i}\omega + v\partial_\chi)^2 + \Omega^2\right] + v^2\gamma\,(\mathrm{i}\omega + v\partial_\chi)g\right\}\psi_\omega\ . \quad (12)$$

Note that one should be careful with the order in the equations above as we are considering nonhomogeneous, i.e., χ-dependent profiles, such that $(\mathrm{i}\omega - v\partial_\chi)$ does not commute with Ω, for example.

B. Conserved generalized inner product and norm

Since we have generalized our physical model to complex fields A and ψ, the Lagrangian density $\mathcal{L}_{\mathrm{pls}}$ is invariant under any transformation of the global phase of the dynamic fields ($A \to \mathrm{e}^{\mathrm{i}\varphi}A$ and $\psi \to \mathrm{e}^{\mathrm{i}\varphi}\psi$). By means of Noether's theorem, this continuous symmetry of $\mathcal{L}_{\mathrm{pls}}$ is related to a conserved current $\partial_\tau\rho + \partial_\chi j = 0$ with the (Noether) charge density (see also Refs. [43, 47])

$$\begin{aligned}\rho &= \mathrm{i}\,(A^*\Pi_{A^*} + \psi^*\Pi_{\psi^*} - \Pi_A A - \Pi_\psi\psi)\\ &= -\operatorname{Im}\left[A^*\,(\partial_\tau A + \gamma g\psi) + \gamma^2\psi^*\,(\partial_\tau - v\partial_\chi)\psi\right] \quad (13)\end{aligned}$$

and the current density

$$j = \operatorname{Im}\left[A^*\,(\partial_\chi A + v\gamma g\psi) + v\gamma^2\psi^*\,(\partial_\tau - v\partial_\chi)\psi\right]. \quad (14)$$

The canonical momentum densities appearing in ρ are given by

$$\Pi_A = \frac{\partial\mathcal{L}_{\mathrm{pls}}}{\partial(\partial_\tau A)} = \frac{1}{2}(\partial_\tau A^* + \gamma g\psi^*) = (\Pi_{A^*})^*\,, \quad (15)$$

$$\Pi_\psi = \frac{\partial\mathcal{L}_{\mathrm{pls}}}{\partial(\partial_\tau\psi)} = \frac{\gamma^2}{2}(\partial_\tau - v\partial_\chi)\psi^* = (\Pi_{\psi^*})^*\,. \quad (16)$$

For stationary modes of the form (9), all time dependencies in ρ and j cancel each other out ($\partial_\tau \to -\mathrm{i}\omega$); that is, these quantities are time independent. The continuity equation consequently simplifies to $\partial_\chi j = 0$, so the current density is a space-time–independent quantity for stationary modes.

The conservation of the total (integrated) Noether charge can be used to derive the conserved, generalized inner product

$$\left\langle\begin{pmatrix}A_1\\ \psi_1\end{pmatrix},\begin{pmatrix}A_2\\ \psi_2\end{pmatrix}\right\rangle = \mathrm{i}\int_{-\infty}^{\infty}\left(A_1^*\Pi_{A_2^*} + \psi_1^*\Pi_{\psi_2^*} - \Pi_{A_1}A_2 - \Pi_{\psi_1}\psi_2\right)\mathrm{d}\chi\ , \quad (17)$$

which is also known as the Klein–Gordon inner product [60], between two arbitrary solutions, (A_1, ψ_1) and (A_2, ψ_2), of the equations of motion in the pulse frame. It has the same properties as usual inner products except for positive definiteness since the product of a field solution (A, ψ) with itself coincides with its total Noether charge,

$$\left\langle\begin{pmatrix}A\\ \psi\end{pmatrix},\begin{pmatrix}A\\ \psi\end{pmatrix}\right\rangle = \int_{-\infty}^{\infty}\rho\,\mathrm{d}\chi\ , \quad (18)$$

which is not necessarily positive but can be any real number. In fact, taking the complex conjugate of Eq. (17) shows that the inner product of A^* and ψ^* with itself has a sign opposite to that of A and ψ. We call this quantity (18) the (pseudo-)norm of the field solution (A, ψ).

IV. JWKB ANALYSIS

As a first approach to understanding the structure of the solutions of the decoupled mode equation (11) in the pulse frame well outside and inside a black hole, we apply the JWKB approximation. That is, we treat the external fields Ω and g as constant ($\partial_\chi\Omega = \partial_\chi g = 0$), so the mode functions ψ_ω are (superpositions of) plane waves, and thus we may set $\partial_\chi \to \mathrm{i}k$ in Eq. (11). The following analysis is thus equivalent to the one in Refs. [43, 46], where a piecewise homogeneous setup is considered. The resulting dispersion relation,

$$(\omega^2 - k^2)\left[\Omega^2 - \gamma^2(\omega + vk)^2\right] + \gamma^2 g^2(\omega + vk)^2 = 0\ , \quad (19)$$

which is just the relation (4) transformed to the pulse frame, can be rearranged into the form

$$\underbrace{\gamma\,(\omega + vk)}_{\omega_{\mathrm{lab}}} = \pm F(k) \quad (20)$$

with the (phase velocity) function

$$F(k) = \Omega\sqrt{1 + \frac{g^2}{\omega^2 - k^2 - g^2}}\ . \quad (21)$$

Each solution $k_\star$ of Eqs. (19) and (20) is an allowed wave vector at the frequency ω. To create a black hole analog as in Fig. 1, however, Ω and/or g must be inhomogeneous. Nevertheless, the (now χ-dependent) wave vector solutions of the (local) dispersion relation will still approximate the physics of the fields well as long as the length scales on which Ω and g vary are much greater than the inverse wave vectors $1/k_\star$.

The dispersion relation (19) has up to four different and possibly complex solutions $k_\star$ for given values of v, Ω, g, and ω. We are particularly interested in the real solutions, which describe propagating waves. The dispersion relation (as a fourth-order polynomial) can be solved analytically, but the resulting expressions are quite lengthy

in general, such that it is hard to grasp their physical properties. Therefore, we will use the form in Eq. (20) to find the solutions graphically instead by plotting both sides of this equation over k. The left-hand side yields a straight line. Note that, according to the Lorentz boost in Eq. (6), $\gamma\,(\omega + vk)$ is the laboratory frame frequency $\omega_{\rm lab}$ of a wave which has the frequency ω and the wave vector k in the pulse frame. For a small $|\omega| < g$, the function $F(k) \geq 0$ appearing on the right-hand side of Eq. (20) is only real for $|k| \geq |\omega|$ and approaches the asymptotic value Ω for $k \to \pm\infty$. At high pulse frame frequencies $|\omega| > g$, on the other hand, F is also real for $|k| < \sqrt{\omega^2 - g^2}$. Solutions $k_\star$ in this k range (intersection points with the straight line $\omega_{\rm lab}$), however, correspond to waves with large laboratory frame frequencies $|\omega_{\rm lab}| > \Omega$ beyond the range of validity of the physical model. Hence, we restrict the analysis to small pulse frame frequencies with $|\omega| < g$ (or even $|\omega| \ll g$).

Examples for the graphical solution of the dispersion relation (including the effects of varying parameters ω and Ω) are depicted in Fig. 2.

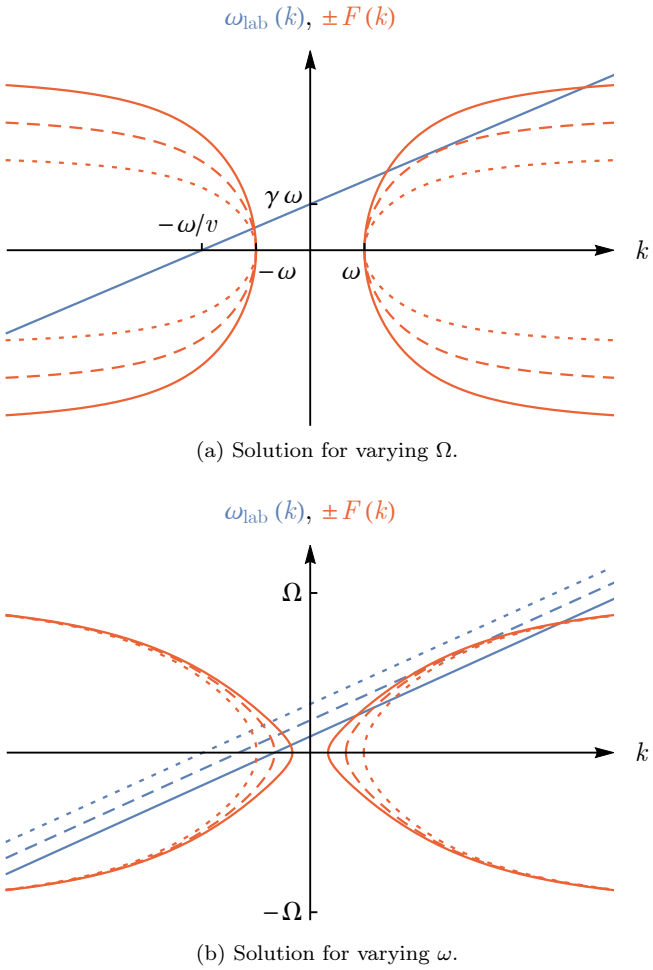

(a) Solution for varying Ω.

(b) Solution for varying ω.

FIG. 2: Graphical solution scheme of the dispersion relation (20) for $v = 1/2$ and constant $g(\chi) = g_0$. In both plots, the straight lines are the graphs of the laboratory frame frequency $\gamma\,(\omega + vk)$, and the curves are the graphs of $\pm F(k)$. (a) Solution for the fixed mode frequency $\omega = g_0/2$ and decreasing Ω (solid $\to$ dashed $\to$ dotted $\pm F$ curves). (b) Solution for constant Ω and increasing ω (solid $\to$ dashed $\to$ dotted $\omega_{\rm lab}$ lines and $\pm F$ curves).

A. Modes outside the black hole

We start to discuss the solutions of the dispersion relation far outside an analog black hole horizon for a low frequency mode $0 < \omega \ll \Omega$. The graphical solution is depicted in Fig. 3. There are four different real solutions: two small wave vectors $k_\star^H \gtrsim \omega$ and $k_\star^{\rm cp} \lesssim -\omega$ as well as two large solutions $k_\star^+ \gg \omega$ and $k_\star^- \ll -\omega$. All four possible wave vectors outside the black hole are thus real (propagating modes). The long-wavelength modes $k_\star^H$ and $k_\star^{\rm cp}$ with wave numbers of the order $\mathcal{O}(\omega)$ are hardly affected by dispersion, whereas the rapidly oscillating modes $k_\star^\pm$ are a consequence of dispersion (they vanish if dispersion is neglected). Let us derive some properties of the modes.

By differentiating the dispersion relation (19) with respect to k (treating ω as a function of k for the moment), we find the expression

$$v_{\rm gr}^{k_\star} = \left.\frac{{\rm d}\omega(k)}{{\rm d}k}\right|_{k=k_\star} = \frac{\partial_k[\pm F(k)]|_{k=k_\star} - v\gamma}{\gamma + \partial_k[\pm F(k)]|_{k=k_\star}\omega/k_\star} \qquad (22)$$

for the pulse frame group velocity of the mode $k_\star$. The $\pm$ sign before F depends on whether $k_\star$ is a plus or minus solution of Eq. (20), i.e., on the sign of the laboratory frame frequency of the mode (vertical coordinate of the corresponding intersection point in Fig. 3). This formula allows us to determine the group velocity signs for all four modes outside the black hole just based on the graphical solution of the dispersion relation in Fig. 3. We find that the group velocities of the modes $k_\star^+$, $k_\star^-$, and $k_\star^{\rm cp}$ are negative, so these modes propagate towards the (stationary) black hole event horizon. The mode $k_\star^{\rm cp}$, which is a low-energy mode (i.e., almost unaffected by dispersion), corresponds to light propagating in the opposite direction as the pulse when viewed from the laboratory frame—that is, this is the counterpropagating mode. (In the sonic black hole analogs based on flowing fluids, this would be the downstream mode.) In the pulse frame, this mode moves towards the black hole and can cross the horizon without being distorted drastically. However, it can also be scattered into an copropagating mode (see Sec. VIII below), but this process is purely classical scattering and does not lead to particle creation. We thus do not expect this mode to be the origin of Hawking radiation. Consequently, we expect $k_\star^\pm$ to be the relevant in-modes for creating the outgoing Hawking radiation as usual in systems with subluminal dispersion (cf., e.g., Refs. [7, 12]). The mode $k_\star^H$ is the only mode with a positive group velocity, so these waves escape the black hole (e.g., Hawking radiation).

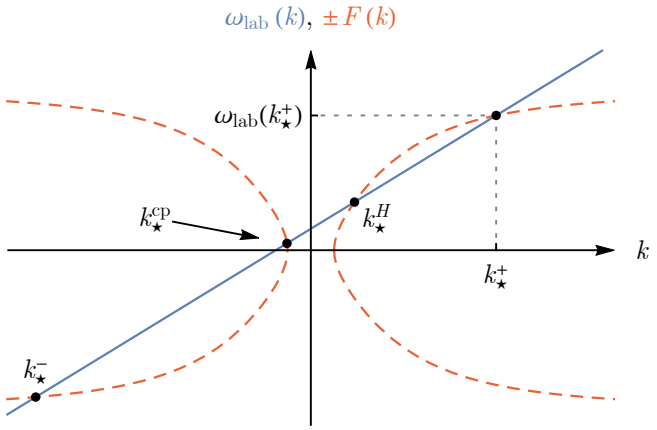

FIG. 3: Graphical solution of the dispersion relation (20) far outside the black hole in Fig. 1, where $v = 2/3$, $g(\chi) = g_0$ is constant, and the local value of Ω is $2g_0$. We consider the mode frequency $\omega = g_0/5$. The straight line is the laboratory frame frequency $\gamma\,(\omega + vk)$. The dashed lines are the graphs of $\pm F(k)$. Here, we get four real solutions (labeled intersection points): the Hawking mode $k_\star^H$, the counterpropagating mode $k_\star^{\rm cp}$, and the two short-wavelength modes $k_\star^\pm$. The vertical value of an intersection point coincides with the frequency of the corresponding wave as measured in the laboratory frame.

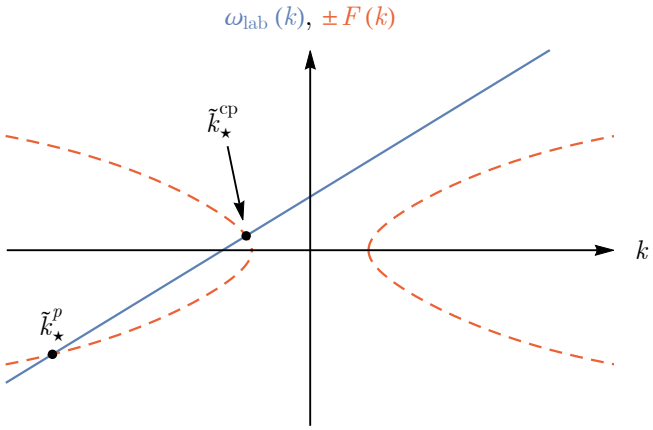

FIG. 4: Graphical solution of the dispersion relation far inside the black hole in Fig. 1. We consider the same configuration as in Fig. 3 except for the value of Ω, which has decreased to $4g_0/5$. The dashed graphs of $\pm F(k)$ have "narrowed" correspondingly, so there are only two real solutions $\tilde{k}_\star^{\rm cp}$ (counterpropagating mode) and $\tilde{k}_\star^p$ (infalling partner) inside the black hole. The two remaining wave vector solutions $\tilde{k}_\star^\pm$ are complex (evanescent modes).

As a next step, we consider the Noether charge densities ρ [see Eq. (13)] of the modes. The mode function A_ω corresponding to a JWKB solution of the (approximate) form $\psi_\omega(\chi) = \exp(\mathrm{i}k_\star\chi - \mathrm{i}\omega\tau)$ is calculated using Eq. (12), with $\partial_\tau \to -\mathrm{i}\omega$ (stationary modes) and $\partial_\chi \to \mathrm{i}k_\star$ (JWKB approximation). The resulting charge density of the mode reads

$$\rho_\omega^{k_\star} = \gamma^2(\omega + vk_\star)\left[1 + \frac{g^2 k_\star\,(v\omega + k_\star)}{(k_\star^2 - \omega^2)^2}\right]. \tag{23}$$

The sign of this charge density depends only on the laboratory frame frequency of the mode,

$$\operatorname{sgn}\rho_\omega^{k_\star} = \operatorname{sgn}(\omega + vk_\star)\ . \tag{24}$$

Hence, it follows from Fig. 3 that $k_\star^-$ is the only mode which propagates a negative Noether charge, so the contribution from this in-mode is the essential ingredient of pair production (cf., e.g., Refs. [5, 7, 9, 11, 12, 15, 17, 18, 43, 47]).

B. Modes inside the black hole

As one goes into the black hole in Fig. 1, Ω decreases, so the graphs of $\pm F(k)$ in the graphical solution in Fig. 3 "narrow" because $F(k) \propto \Omega$; cf. Fig. 2(a). The solutions $k_\star^H$ and $k_\star^+$ will thus approach each other and merge at a certain point on the way towards the horizon, at which point the straight line $\gamma\,(\omega + vk)$ is tangent to $F(k)$—see the dashed $\pm F(k)$ curves in Fig. 2(a). Beyond this point, these two real solutions become two complex solutions, $\tilde{k}_\star^+$ and $\tilde{k}_\star^- = (\tilde{k}_\star^+)^*$, with $\operatorname{Im}\tilde{k}_\star^+ > 0$, so the Hawking mode escaping the black hole disappears beyond this "point of no return", which behaves like a frequency-specific event horizon. The allowed wave vectors vary rapidly around this point, so the JWKB approximation breaks down there. Note that, in the limit $\omega \to 0$, the point of no return coincides with the ("absolute") event horizon since low-frequency waves travel at the fastest speed (subluminal dispersion). Deep inside the black hole in Fig. 1, the JWKB approximation is valid again. See Fig. 4 for the graphical solution of the local dispersion relation. Both real solutions, $\tilde{k}_\star^{\rm cp}$ and $\tilde{k}_\star^p$, describe modes with negative group velocities according to Eq. (22), so they propagate deeper into the black hole (as expected inside the event horizon). The mode $\tilde{k}_\star^{\rm cp}$ has a positive Noether charge density while $\tilde{k}_\star^p$ carries negative charge. We conclude that $\tilde{k}_\star^{\rm cp} \approx k_\star^{\rm cp}$ is the counterpropagating mode, which crossed the horizon and is now inside the black hole. The second mode, $\tilde{k}_\star^p$, with a negative laboratory frame frequency (negative energy) is the infalling partner mode of the outgoing Hawking mode $k_\star^H$; see, e.g., Refs. [2, 5]. The mode structure inside the black hole is thus as expected according to Refs. [5, 7, 9, 11, 12, 15, 17, 18, 43, 47] again.

One of the standard ways to derive the Hawking effect is to trace a late-time outgoing Hawking wave packet back in time in order to find the early-time ingoing wave packets the Hawking packet is composed of initially (see, e.g., Ref. [7]). Since there are no solutions inside the black hole which can approach the horizon (subluminal dispersion), the relevant boundary condition for that derivation of Hawking radiation is that the mode function vanishes

deep inside the black hole (i.e., the mode is evanescent). In the limit of wave packets which are sharply peaked around a unique frequency ω, the wave packets become very extended in space and time—that is, we consider single stationary modes. We have to make sure that the mode function ψ_ω satisfies the boundary condition; however, a function ψ_ω which is nonzero outside the black hole cannot vanish identically everywhere inside the horizon [7]. We therefore demand ψ_ω to decay rapidly (exponentially) inside the black hole. In terms of the JWKB solutions explained above, that means that only the complex wave vector $\tilde{k}_\star^-$ may contribute to ψ_ω beyond the horizon since $|\exp(\mathrm{i}\tilde{k}_\star^-\chi - \mathrm{i}\omega\tau)| = \exp(-\chi \operatorname{Im}\tilde{k}_\star^-)$ and $\operatorname{Im}\tilde{k}_\star^- < 0$, so this function decays rapidly along the way deeper into the black hole (decreasing χ). However, we cannot continue this mode function across the event horizon using the JWKB technique because this approximation breaks down in the vicinity of the horizon (at least in the coordinates we use here; see also Ref. [59]).

V. CONNECTION OF JWKB SOLUTIONS ACROSS THE EVENT HORIZON

In order to continue a mode function ψ_ω, which decays exponentially inside the event horizon (according to the boundary condition mentioned above), into the exterior region of the black hole, we have to take the full decoupled mode equation (11) into account. The complexity of this equation depends on the concrete pulse shape given by $\Omega(\chi)$ and $g(\chi)$. As already mentioned in Sec. II, we assume that $g(\chi) = g_0$ is constant (see also Fig. 1). We thus need to specify $\Omega(\chi)$.

We want to model the Schwarzschild metric with

$$\mathfrak{g}_{00} = 1 - \frac{2G_\mathrm{N}M}{r} \ . \tag{25}$$

This metric has a horizon at $r = 2G_\mathrm{N}M$ (the Schwarzschild radius), a singularity at $r = 0$, and becomes asymptotically flat for $r \to \infty$. For the dielectric black hole analog, the $\mathfrak{g}_{00}$ component behaves as

$$\mathfrak{g}_{00}^\mathrm{eff} \propto 1 - \frac{v^2}{c_\mathrm{low}^2(\chi)} = 1 - v^2\left(1 + \frac{g_0^2}{\Omega^2(\chi)}\right); \tag{26}$$

see also Eq. (62) below. Note that $c_\mathrm{low}^2(\chi)$ refers to the low-energy limit in Eq. (5) where the analogy to gravity applies. In order to model the Schwarzschild metric, we assume the following profile (with some constant $\xi > 0$):

$$\Omega(\chi) = \Omega_0\sqrt{1 + 2\xi\chi} \ , \quad g(\chi) = g_0 \ . \tag{27}$$

For simplicity, we choose χ such that the horizon is located at $\chi = 0$, so the black hole exterior region is $\chi > 0$ and the interior region is $\chi < 0$. At the horizon $\chi = 0$, we have $\mathfrak{g}_{00}^\mathrm{eff} = 0$, which translates to the condition (7), leading to the relation

$$\Omega_0 = v\gamma g_0 \ . \tag{28}$$

The slope $\mathrm{d}c_\mathrm{low}(\chi)/\mathrm{d}\chi$ at the horizon determines the surface gravity (remember that v is constant), which in turn sets the Hawking temperature; see Eqs. (55) and (63) below. Similarly to the Schwarzschild metric, where the strength of the gravitational field vanishes at $r \to \infty$, the polarizability of the medium goes to zero as $\chi \to \infty$. Furthermore, the refractive index diverges (formally) for $\chi = -1/(2\xi)$, which is similar to the singularity at $r = 0$. Of course, such a profile (27) is not a realistic model for a real laser pulse, but—as we shall see below—it allows us to derive an exact solution of the mode equation in analogy to Ref. [14]. Furthermore, because only the vicinity of the horizon is relevant for the creation of low-energy Hawking radiation, we can interpret this profile (27) as an approximation of a realistic pulse profile in the region near the horizon $\xi|\chi| \ll 1$. In terms of a Taylor expansion $\Omega^2(\chi) = \Omega_0^2 + 2\Omega_0^2\xi\chi + \mathcal{O}(\chi^2)$, we neglect the higher-order terms $\mathcal{O}(\chi^2)$ since $\Omega^2(\chi)$ is supposed to be slowly varying. For example, since the modes we are interested in decay rapidly inside the black hole, they do not see the singularity at $\chi = -1/(2\xi)$, so that this approximation should be reasonable. Since the Hawking temperature is supposed to be sufficiently low, the JWKB approximation will be valid at both edges (inside and outside the black hole) of the linearized region. This way, we can continue a JWKB solution inside the black hole across the horizon using the linearized mode equation.

Inserting the pulse profile (27) into the general decoupled mode equation (11) yields the equation

$$\begin{aligned}\left\{(\omega^2 + \partial_\chi^2)\left[(\mathrm{i}\omega + v\partial_\chi)^2 + v^2g_0^2\,(1 + 2\xi\chi)\right]\right.\\ \left. - g_0^2\,(\mathrm{i}\omega + v\partial_\chi)^2\right\}\psi_\omega = 0 \ .\end{aligned} \tag{29}$$

In this section, we will study the solutions of this mode equation in the positive frequency range $0 < \omega \lesssim \xi$, which covers the essential part of the Hawking spectrum. The corresponding negative-frequency solutions can be derived by complex conjugation. The solution scheme via transformation to momentum space and contour integration is analogous to Refs. [9–12, 17, 47], for example.

A. Solution of the mode equation

Equation (29) can be solved in reciprocal (momentum) space. To this end, we Fourier–Laplace transform the equation by inserting

$$\psi_\omega(\chi) = \int_\mathcal{C} \tilde{\psi}_\omega(k)\mathrm{e}^{\mathrm{i}k\chi}\,\mathrm{d}k \tag{30}$$

with the (yet unspecified) complex integration contour $\mathcal{C}$. By means of this transform, the fourth-order differential equation (29) in χ becomes the first-order differential

equation in k ($\partial_\chi \to \mathrm{i}k$ and $\chi \to \mathrm{i}\partial_k$),

$$\partial_k \tilde{\psi}_\omega(k) = \frac{1}{2\mathrm{i}v^2 g_0^2 \xi}\left[\left(1+\frac{g_0^2}{k^2-\omega^2}\right)(\omega+vk)^2 - v^2 g_0^2\right] \times \tilde{\psi}_\omega(k) \ , \quad (31)$$

which is easy to solve for $\tilde{\psi}_\omega(k)$. After transforming back to position space via Eq. (30), the solution reads

$$\psi_\omega(\chi) = \int_{\mathcal{C}} f(k) \mathrm{e}^{\chi h(k)} \, \mathrm{d}k \ , \quad (32)$$

with the two auxiliary functions

$$f(k) = \left[\mathrm{i}\left(\frac{k}{\omega}-1\right)\right]^{-\mathrm{i}\,(1+v)^2\omega/(4v^2\xi)} \times \left[\mathrm{i}\left(\frac{k}{\omega}+1\right)\right]^{\mathrm{i}\,(1-v)^2\omega/(4v^2\xi)} \quad (33)$$

and

$$h(k) = \mathrm{i}k\left(1 - \frac{v^2k^2/3 + v\omega k + \omega^2}{2v^2 g_0^2 \xi \chi}\right). \quad (34)$$

The constant of integration, which is irrelevant for the Hawking spectrum, is related to the contour $\mathcal{C}$ and has been omitted for simplicity. Note that the exponent in Eq. (32) can be cast into the form

$$\chi h(k) = \mathrm{i}k\chi - \mathrm{i}\,\frac{(k+\omega/v)^3}{6g_0^2\xi} + \mathrm{i}\,\frac{\omega^3}{6v^3 g_0^2 \xi} \ , \quad (35)$$

where the last term can be absorbed by the integration constant mentioned above.

Equation (32) is a contour integral representation of the mode function ψ_ω. In order to define complex powers as in $f(k)$, we have to specify the two branch cuts of the complex natural logarithm starting at the two singularities $k = \pm\omega$. Here, we choose these branch cuts to run upwards in the complex plane (parallel with respect to the positive imaginary axis). This corresponds to the principal value $\mathrm{Ln}\,\mathfrak{z}$ of the complex natural logarithm (i.e., $-\pi < \mathrm{Im}[\mathrm{Ln}\,\mathfrak{z}] \leq \pi$). As we shall see below, this choice is most convenient for deriving mode functions which satisfy the required boundary condition, that is, are evanescent inside the black hole. With other choices, we can derive other solutions of the wave equation (e.g., with a contribution from the partner mode inside).

B. Mode function inside the black hole ($\chi < 0$): Boundary condition

Let us first consider the mode function ψ_ω in Eq. (32) inside the black hole, where we have imposed the boundary condition for the derivation of the Hawking effect according to Sec. IV B. This boundary condition is fulfilled by selecting the (end points of the) integration contour $\mathcal{C}$ appropriately. The contour can "safely" run to infinity into any direction of the complex plane where the exponential part of the integrand, $\exp[\chi h(k)]$, decays to zero; that is, $\mathrm{Re}[\chi h(k)] \to -\infty$, while the function $f(k)$ is unproblematic. These "valleys" of the integrand are located at

- $\pi/3 < \mathrm{Arg}\,k < 2\pi/3$ (top),
- $-\pi < \mathrm{Arg}\,k < -2\pi/3$ (bottom left), and
- $-\pi/3 < \mathrm{Arg}\,k < 0$ (bottom right).

For other directions (i.e., between these valleys), $|\exp[\chi h(k)]|$ diverges for $|k| \to \infty$.

Here, we choose to integrate just below the real axis from $-\infty$ to ∞, that is, from the bottom-left valley into the bottom-right one and below the singularities at $k = \pm\omega$, so we have fixed the contour $\mathcal{C}$ appearing in Eqs. (30) and (32). We can still, however, deform the integration contour by means of Cauchy's theorem in order to simplify the integration without changing the value of the integral. The exponent function $h(k)$ in the integrand has two saddle points, which satisfy $h'(k_s) = 0$. For $\chi < 0$, these saddle points are

$$\tilde{k}_s^\pm = \pm\mathrm{i}g_0\sqrt{-2\xi\chi} - \frac{\omega}{v} \ . \quad (36)$$

The saddle point $\tilde{k}_s^-$ connects the two adjacent valleys in the lower complex half plane (bottom left and right) with each other. Hence, we may deform $\mathcal{C}$ smoothly (keeping the end points fixed) without ever encountering any singularities or branch cuts of the integrand so that the final contour $\mathcal{C}_{\mathrm{in}}$ runs through $\tilde{k}_s^-$ along the "mountain pass route"; see Fig. 5. The contribution from the saddle point $\tilde{k}_s^-$ will dominate the value of the integral since the rest of the integration runs through the valleys.

The other saddle point $\tilde{k}_s^+$ corresponds to a "mountain pass" which connects the upper (top) valley with the two lower (bottom) valleys with a bifurcation point near the origin. The height of this pass increases exponentially for increasing $|\chi|$, but our selected contour does not go through this point.

Applying the saddle point method (see, e.g., Ref. [61]), the mode function $\psi_\omega(\chi < 0) \approx \psi_\omega^{\mathrm{inside}}(\chi)$ inside the black hole is thus approximately given by the saddle point contribution from $\tilde{k}_s^-$. The leading-order term of the saddle point expansion (which becomes asymptotically exact in the formal limit $\chi \to -\infty$) reads

$$\psi_\omega^{\mathrm{inside}}(\chi) = \sqrt{\frac{2\pi}{|\chi h''(\tilde{k}_s^-)|}} f(\tilde{k}_s^-) \mathrm{e}^{\chi h(\tilde{k}_s^-)} \ . \quad (37)$$

The higher-order corrections of the saddle point expansion are negligible if

$$|\xi\chi|^{3/2} \gg \frac{\gamma}{v}\frac{\xi}{\Omega_0} = \frac{\xi}{v^2 g_0} \ . \quad (38)$$

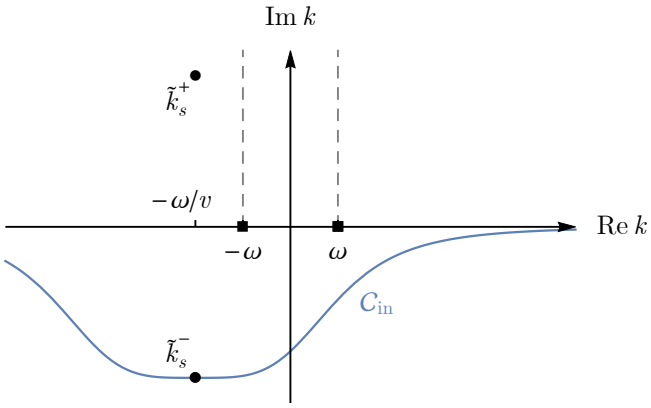

(a) Integration contour $\mathcal{C}_{\rm in}$ (schematic).

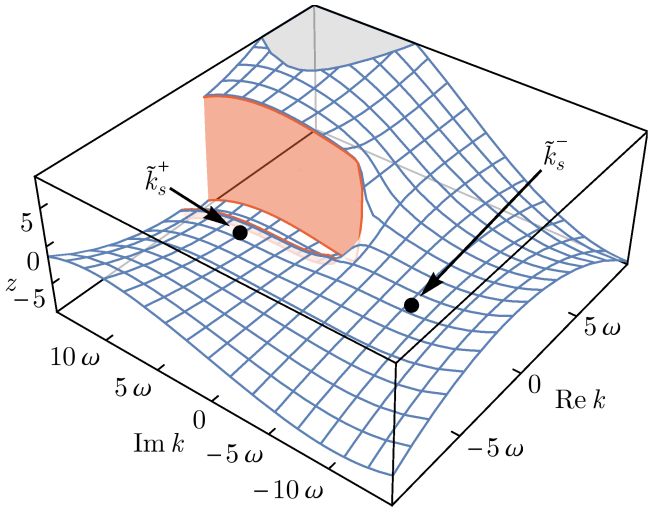

(b) Absolute value (logarithmic) of the integrand.

FIG. 5: Contour integration (32) inside the black hole ($\chi < 0$). (a) Integration contour $\mathcal{C}_{\rm in}$ running through the saddle point $\tilde{k}_s^-$ (not drawn to scale). The squares mark the singularities of the integrand due to the complex powers in $f(k)$, and the dashed lines are the corresponding branch cuts. (b) Logarithmic landscape plot of the absolute value of the integrand, i.e., $z = \ln|f(k)e^{\chi h(k)}|$ over a complex k. The parameter values applied in this plot ($v = 1/2$, $\xi = \omega = g_0/10$, and $\chi = -3/g_0$, so $\Omega \approx 0.4 g_0$) are not within the validity range (38) of the saddle point approximation but have been chosen for illustrative purposes. We see that the saddle point $\tilde{k}_s^-$ connects the two valleys of the integrand in the lower complex half plane.

For the derivation of this inequality, we have used that the typical frequency of Hawking radiation $\omega \lesssim \mathcal{O}(\xi)$ is set by the surface gravity. Since g_0 and Ω_0 are characteristic scales of the medium and thus are supposed to be much larger than ξ (and ω), the right-hand side of Eq. (38) is very small. Sufficiently far inside the black hole as determined by the condition (38), the mode function $\psi_\omega(\chi < 0)$ is therefore approximated well by the leading-order term (37). However, we want to stay away from the singularity, so we assume $\xi|\chi| \ll 1$. Hence ξ has to be small enough so that both assumptions can be satisfied simultaneously (low Hawking temperature).

Let us check to see whether $\psi_\omega^{\rm inside}$ does indeed satisfy the required boundary condition. We evaluate the absolute value of Eq. (37) to find

$$|\psi_\omega^{\rm inside}(\chi)| = \sqrt[4]{\frac{2\pi^2 g_0^2 \xi}{|\chi|}}\, |f(\tilde{k}_s^-)| e^{-2g_0|\chi|\sqrt{2\xi|\chi|}/3} \propto \frac{e^{-2g_0|\chi|\sqrt{2\xi|\chi|}/3}}{\sqrt[4]{|\chi|}}\,, \tag{39}$$

so the mode function decays exponentially beyond the horizon, and hence the integration contour is in accordance with the boundary condition. For values of χ satisfying the condition (38), we thus find that $|\psi_\omega^{\rm inside}(\chi)|$ is suppressed exponentially.

Note that the contribution from the other saddle point $\tilde{k}_s^+$ would instead grow exponentially when going further and further inside the black hole—which explains why we selected our contour in such a way that it does not go through this saddle point.

C. Mode function outside the black hole ($\chi > 0$): Identification of the JWKB modes

Now that we know the correct integration contour, we evaluate the contour integral (32) outside the black hole in order to calculate the analytically continued mode function $\psi_\omega(\chi > 0)$. However, for $\chi > 0$, the saddle points of $h(k)$ have moved to the positions

$$k_s^\pm = \pm g_0\sqrt{2\xi\chi} - \frac{\omega}{v} \tag{40}$$

on the real axis, so $\mathcal{C}_{\rm in}$ is not the most advantageous integration contour for $\chi > 0$. The validity condition (38) for the saddle point approximation (which we want to apply again) implies that χ must be large enough that $|k_s^\pm| \gg \omega$, which means that the singularities of the integrand at $k = \pm\omega$ are between k_s^- and k_s^+. The saddle point k_s^- connects the bottom-left valley (where the integration contour starts) with the top valley in the upper complex half plane. The other saddle point k_s^+ leads from this valley into the bottom-right valley where the integration ends. Hence, we deform $\mathcal{C}_{\rm in}$ again, always avoiding going across any nonholomorphic regions of the integrand, so that the final contour $\mathcal{C}_{\rm out}$ follows the path of steepest descent through the saddle points. The top valley, which $\mathcal{C}_{\rm out}$ must traverse, however, is divided by the branch cuts, so the contour must circumvent these two discontinuous half lines in the complex plane as depicted in Fig. 6. Note that, in contrast to Ref. [47], we do not neglect any branch cuts. Putting all dominant contributions to the integral together, the mode function outside the black hole is thus composed of the saddle point contributions $\psi_\omega^\pm$ and the functions $\psi_\omega^{\rm cut\pm}$, which

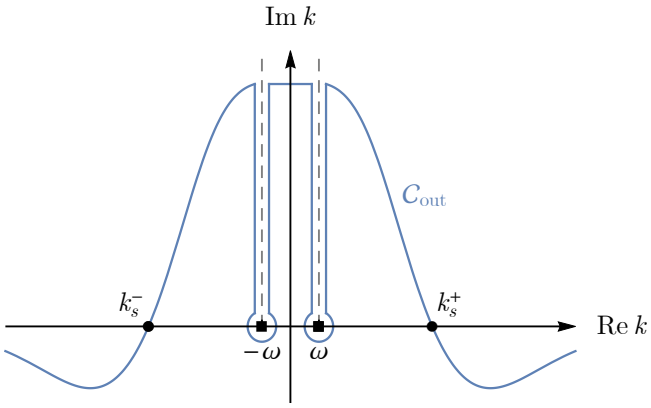

(a) Integration contour $\mathcal{C}_{\text{out}}$ (schematic).

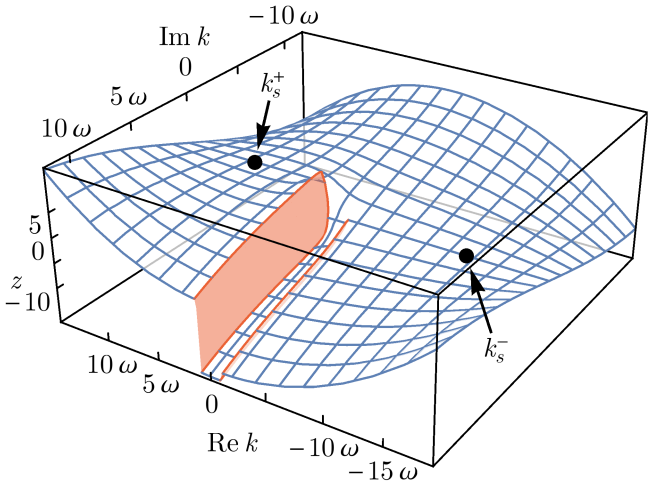

(b) Absolute value (logarithmic) of the integrand.

FIG. 6: Contour integration (32) outside the black hole ($\chi > 0$). (a) Deformed integration contour $\mathcal{C}_{\text{out}}$ running through the saddle points $k_s^\pm$ and circumventing the branch cuts. This sketch is not drawn to scale and the saddle points are drawn symmetrically around zero (not $-\omega/v$) for simplicity. (b) Landscape plot of the integrand, i.e., $z = \ln|f(k)\mathrm{e}^{\chi h(k)}|$ over $k \in \mathbb{C}$, for the same system as in Fig. 5(b) ($v = 1/2$, $\xi = \omega = g_0/10$) but outside the horizon at $\chi = 5/g_0$, where $\Omega \approx 0.8 g_0$. Note that the discontinuity of the branch cut at $\mathrm{Re}\,k = +\omega$ is significantly larger than that at $\mathrm{Re}\,k = -\omega$, which makes the latter a bit hard to notice.

are due to the circumvention of the branch cuts originating from $k = \pm\omega$,

$$\psi_\omega(\chi > 0) \approx \psi_\omega^-(\chi) + \psi_\omega^{\text{cut}-}(\chi) + \psi_\omega^{\text{cut}+}(\chi) + \psi_\omega^+(\chi)\,. \tag{41}$$

Let us now identify the four JWKB modes which have been explained in Sec. IV A in this mode function.

The leading-order saddle point contributions read

$$\psi_\omega^\pm(\chi) = \mathrm{e}^{\mp\mathrm{i}\pi/4}\sqrt[4]{\frac{2\pi^2 g_0^2\xi}{\chi}}\,\mathrm{e}^{\chi h(k_s^\pm)}\,\mathrm{e}^{\pm\pi\omega/(2v\xi)} \times\left|\frac{k_s^\pm}{\omega}-1\right|^{-\mathrm{i}(1+v)^2\omega/(4v^2\xi)}\left|\frac{k_s^\pm}{\omega}+1\right|^{\mathrm{i}(1-v)^2\omega/(4v^2\xi)}. \tag{42}$$

These functions oscillate rapidly due to the large saddle point values $|k_s^\pm| \sim g_0\sqrt{2\xi\chi} \gg \omega$ as implied by inequality (38) and $\xi\chi \ll 1$. For large χ, these expressions become exact solutions of the decoupled mode equation (29), so they are asymptotic independent modes and should therefore coincide with two JWKB modes in this limit. Solving the local dispersion relation (19) for the current pulse profile (27) and large wave vectors (neglecting ω) yields two solutions $k_\star \approx \pm g_0\sqrt{2\xi\chi}$, which are asymptotically equal to the saddle points $k_s^\pm$. Hence, the modes $\psi_\omega^\pm$ correspond (asymptotically) to the JWKB modes $k_\star^\pm$.

Now we consider the branch cut contributions. The contour $\mathcal{C}_{\text{out}}$ may run arbitrarily deep into the top valley (where the integrand is exponentially suppressed), so we integrate infinitesimally close on both sides along the cuts, respectively, up to infinity. The small circles around the singularities in Fig. 6(a) do not yield any contributions. After some substitutions, the resulting (exact) integrals can be written

$$\psi_\omega^{\text{cut}\pm}(\chi) = \pm 2\mathrm{i}\sinh\left[\frac{\pi\,(1\pm v)^2\omega}{4v^2\xi}\right]\int_0^\infty\left(\frac{u}{\omega}\right)^{\mp\mathrm{i}\frac{(1\pm v)^2\omega}{4v^2\xi}} \times\left(-\frac{u}{\omega}\pm 2\mathrm{i}\right)^{\pm\mathrm{i}(1\mp v)^2\omega/(4v^2\xi)}\mathrm{e}^{\chi h(\mathrm{i}u\pm\omega)}\,\mathrm{d}u\,. \tag{43}$$

As with the saddle point contributions, we can uniquely identify $\psi_\omega^{\text{cut}\pm}$ with JWKB modes, respectively, in the limit $\chi \to \infty$. The integrand in Eq. (43) can be substantially simplified for a large χ because then only small values $u \ll \omega$ are significant for the integration. We can express the remaining integral by the gamma function Γ. The resulting mode functions read

$$\psi_\omega^{\text{cut}\pm}(\chi) \sim \omega\,(\pm 2\mathrm{i})^{1\pm\mathrm{i}(1\mp v)^2\omega/(4v^2\xi)}\sinh\left[\frac{\pi\,(1\pm v)^2\omega}{4v^2\xi}\right] \times\Gamma\left[1\mp\frac{\mathrm{i}\,(1\pm v)^2\omega}{4v^2\xi}\right]\left(\frac{1}{\omega\chi}\right)^{1\mp\mathrm{i}(1\pm v)^2\omega/(4v^2\xi)}\mathrm{e}^{\pm\mathrm{i}\omega\chi}\,. \tag{44}$$

This is the leading-order asymptotic term of the exact integral in Eq. (43), so it consequently solves the decoupled mode equation (29) in the limit $\chi \to \infty$. These functions do still solve the mode equation for $\chi \to \infty$ if dispersion is neglected, that is, if we discard all terms containing third- or higher-order derivatives acting on the ψ field ($\omega^n\partial_\chi^m$, with $n + m > 2$ since ω originates from a time

derivative ∂_τ). The modes described by $\psi_\omega^{\mathrm{cut}\pm}$ are thus only slightly affected by dispersion far outside the black hole and correspond to the Hawking mode $k_\star^H$ and the counterpropagating mode $k_\star^{\mathrm{cp}}$. The phase/group velocity of $\psi_\omega^{\mathrm{cut}+}$ is positive, so this mode propagates away from the black hole and can therefore be identified with the Hawking mode. The other branch cut contribution $\psi_\omega^{\mathrm{cut}-}$ has a negative group velocity, so it corresponds to the counterpropagating mode.

D. Current densities

For the derivation of the Hawking spectrum, we need to know the contribution from the positive- and negative-norm in-modes ($k_\star^+$ and $k_\star^-$ in the JWKB picture) to the outgoing Hawking radiation. In the time-independent limit (stationary modes), we therefore have to calculate the Noether charge current densities $j_\omega^\pm$ of the modes $\psi_\omega^\pm$ using Eqs. (12) and (14), with $\partial_\tau \to -\mathrm{i}\omega$. The current density of a stationary mode is exactly constant (see Sec. III B), so we may calculate $j_\omega^\pm$ very far outside the black hole ($\chi \to \infty$) where all χ-dependent terms in $j_\omega^\pm$ vanish. (These terms are artifacts caused by the saddle point approximation anyway.) The resulting current densities assume the simple form

$$j_\omega^\pm = \mp 2\pi\Omega_0^2\xi\, \mathrm{e}^{\pm\pi\omega/(v\xi)} \ . \tag{45}$$

The current density $j_\omega^{\mathrm{cut}+}$ associated with the branch cut contribution $\psi_\omega^{\mathrm{cut}+}$ (Hawking mode), which we also need to know for deriving the Hawking spectrum, is calculated in the same way as $j_\omega^\pm$ above. The result reads

$$j_\omega^{\mathrm{cut}+} = 2\pi\Omega_0^2\xi \left[\mathrm{e}^{\pi\omega/(v\xi)} - \mathrm{e}^{-\pi\,(1+v^2)\omega/(2v^2\xi)}\right] . \tag{46}$$

Of course, the current density of the exponentially decaying mode inside the black hole vanishes.

VI. HAWKING SPECTRUM

We are now in the position to calculate the Hawking spectrum. Here, we only present a brief review of the derivation of the Hawking effect. For a more detailed explanation, we refer the reader to Ref. [7], for example.

The Hawking effect requires a quantum-field-theoretic framework, so the classical fields A and ψ are substituted by Hermitian field operators $\hat{\mathfrak{A}}$ and $\hat{\Psi}$, which obey the bosonic equal-time commutation relations and solve the same equations of motion as the classical fields. Hence, the Klein–Gordon inner product (17) continues to be useful in the context of the quantized fields. We find

$$\left[\left\langle \begin{pmatrix} A_1 \\ \psi_1 \end{pmatrix}, \begin{pmatrix} \hat{\mathfrak{A}} \\ \hat{\Psi} \end{pmatrix} \right\rangle, \left\langle \begin{pmatrix} A_2 \\ \psi_2 \end{pmatrix}, \begin{pmatrix} \hat{\mathfrak{A}} \\ \hat{\Psi} \end{pmatrix} \right\rangle\right] = -\left\langle \begin{pmatrix} A_1 \\ \psi_1 \end{pmatrix}, \begin{pmatrix} A_2^* \\ \psi_2^* \end{pmatrix} \right\rangle \tag{47}$$

(cf. Ref. [7]), where $[\cdot,\cdot]$ denotes the commutator and (A_n, ψ_n) are two arbitrary, classical field solutions of the equations of motion. The inner product allows us to "project" the field operators onto a set of classical field solutions (mode expansion), and Eq. (47) facilitates the derivation of the corresponding annihilation and creation operators $\hat{\mathfrak{a}}$ and $\hat{\mathfrak{a}}^\dagger$. As one may infer from the above commutator, positive-norm modes correspond to annihilation operators, while negative-norm modes correspond to creation operators.

As explained in Sec. IV B, a late-time outgoing Hawking wave (packet) originates from contributions from the three in-modes $k_\star^\pm$ and $k_\star^{\mathrm{cp}}$ at early times. For stationary modes (time-independent picture) and expressed via creation and annihilation operators, this statement reads

$$\hat{\mathfrak{a}}_\omega^H = \alpha_\omega \hat{\mathfrak{a}}_\omega^+ + \beta_\omega (\hat{\mathfrak{a}}_\omega^-)^\dagger + \eta_\omega \hat{\mathfrak{a}}_\omega^{\mathrm{cp}} \tag{48}$$

with the Bogoliubov coefficients α_ω, β_ω, and η_ω. As explained above, the rapidly oscillating, negative-norm mode is represented by a creation operator $(\hat{\mathfrak{a}}_\omega^-)^\dagger$ in this relation. Since the above operators obey the usual commutation relations for bosonic creation and annihilation operators, we obtain the (unitarity) relation

$$|\alpha_\omega|^2 - |\beta_\omega|^2 + |\eta_\omega|^2 = 1 \ . \tag{49}$$

Note that this equality can also be derived from the properties of the classical solutions of the wave equation. In terms of the current densities, this relation corresponds to charge conservation

$$j_\omega^+ + j_\omega^- + j_\omega^{\mathrm{cut}-} + j_\omega^{\mathrm{cut}+} = 0 \ . \tag{50}$$

Here the saddle point contribution j_ω^+ from k_s^+ corresponds to $|\alpha_\omega|^2$, while the other one, j_ω^- from k_s^-, is associated with $|\beta_\omega|^2$. Furthermore, the two branch cut contributions $j_\omega^{\mathrm{cut}-}$ and $j_\omega^{\mathrm{cut}+}$ correspond to the counterpropagating mode (i.e., $|\eta_\omega|^2$) and the Hawking mode, respectively. Note that ρ_ω^- is negative, while the other three, ρ_ω^+, $\rho_\omega^{\mathrm{cut}-}$, and $\rho_\omega^{\mathrm{cut}+}$, are positive; see Eq. (24). However, since only the Hawking mode $\psi_\omega^{\mathrm{cut}+}$ has a positive group velocity (away from the horizon) while the other three are negative (towards the horizon), we find that $j_\omega^{\mathrm{cut}+}$ and j_ω^- are positive, while $j_\omega^{\mathrm{cut}-}$ and j_ω^+ are negative. Altogether, with the correct normalization, we have the following identifications:

- $|\alpha_\omega|^2 \to -j_\omega^+/j_\omega^{\mathrm{cut}+}$,
- $|\beta_\omega|^2 \to +j_\omega^-/j_\omega^{\mathrm{cut}+}$, and
- $|\eta_\omega|^2 \to -j_\omega^{\mathrm{cut}-}/j_\omega^{\mathrm{cut}+}$.

We assume the in-vacuum state for the fields in the dielectric medium. This quantum state is defined by

$$\hat{\mathfrak{a}}_\omega^+ |0_{\mathrm{in}}\rangle = \hat{\mathfrak{a}}_\omega^- |0_{\mathrm{in}}\rangle = \hat{\mathfrak{a}}_\omega^{\mathrm{cp}} |0_{\mathrm{in}}\rangle = 0 \ , \tag{51}$$

so there are no particles initially. Using Eq. (48), the mean number of Hawking particles emitted (per unit time) from the in-vacuum state turns out to be

$$\langle 0_{\mathrm{in}} \,|\, (\hat{\mathfrak{a}}_\omega^H)^\dagger \hat{\mathfrak{a}}_\omega^H \,|\, 0_{\mathrm{in}} \rangle = \langle \hat{\mathfrak{n}}_\omega^H \rangle_{\mathrm{in}} = |\beta_\omega|^2 \ , \tag{52}$$

which is the quantity we are interested in.

For stationary modes, Eq. (52) can be evaluated by means of the current densities j_ω of the individual modes, which describe the propagation of the conserved Noether charge. The Hawking particle yield is given by the relative amount of negative charge contribution j_ω^- from the negative-norm in-mode to the outgoing Hawking flux $j_\omega^{\text{cut}+}$. We already calculated these current densities; see Eqs. (45) and (46). From Eq. (45) and the above identification, we may infer

$$\left|\frac{j_\omega^-}{j_\omega^+}\right| = \frac{|\beta_\omega|^2}{|\alpha_\omega|^2} = \exp\!\left(-\frac{2\pi\omega}{v\xi}\right). \tag{53}$$

Exploiting the unitarity relation (49), we find

$$|\beta_\omega|^2 = \frac{1-|\eta_\omega|^2}{\mathrm{e}^{2\pi\omega/(v\xi)}-1} = \frac{\Gamma_\omega}{\mathrm{e}^{\omega/T_\mathrm{H}}-1} \tag{54}$$

with the Hawking temperature

$$T_\mathrm{H} = \frac{v\xi}{2\pi} \tag{55}$$

and the frequency-dependent gray-body factor

$$\Gamma_\omega = 1-|\eta_\omega|^2 \ , \tag{56}$$

which can be determined by comparing $j_\omega^-/j_\omega^{\text{cut}+}$ (yielding $|\beta_\omega|^2$) with the above expression:

$$\Gamma_\omega = \frac{2\sinh[\pi\omega/(v\xi)]}{\mathrm{e}^{\pi\omega/(v\xi)}-\mathrm{e}^{-\pi(1+v^2)\omega/(2v^2\xi)}} \ . \tag{57}$$

As expected, this factor is bounded from above and below via $0<\Gamma_\omega<1$ and approaches unity for $\omega/\xi\to\infty$ and also for $v\to 1$. For $\omega/\xi\to 0$, it converges to a finite value $4v/(1+v)^2<1$. For a small ω, the spectrum thus behaves as $1/\omega$—the same scaling that was found in Ref. [43] for a step-function profile.

A. Transformation to the laboratory frame

As a final step, we derive the frequency spectrum of Hawking radiation as measured in the laboratory. We thus have to express the pulse frame quantities ω and ξ in terms of laboratory frame quantities.

Let us start with the frequency ω. Asymptotically (large χ), a Hawking wave with the frequency $\omega>0$ in the pulse frame oscillates with the wave vector $k=+\omega$; see for example the functional form of $\psi_\omega^{\text{cut}+}$ in Eq. (44). According to the Lorentz boost (6), this wave has the frequency

$$\omega_\mathrm{lab} = \gamma\,(1+v)\,\omega \tag{58}$$

in the laboratory frame. This equation allows us to express ω in the Hawking spectrum in terms of ω_lab.

The surface-gravity-like quantity ξ has been defined as the value of $(\partial_\chi\Omega)/\Omega$ at the horizon $\chi=0$ in Sec. V. Hence, the corresponding quantity ξ_lab in the laboratory frame (according to which the horizon is located at $x=vt$) is Lorentz contracted, as proven by

$$\xi_\mathrm{lab} = \left.\frac{\partial_x\Omega}{\Omega}\right|_{x-vt=0} = \gamma\xi \ , \tag{59}$$

where we have inserted the pulse shape (27) in laboratory frame coordinates.

VII. EFFECTIVE METRIC

Now let us discuss the analogy to gravity. If we assume slowly varying fields and thus neglect higher-order time derivatives, we may insert the approximate solution $\psi\approx g\partial_t A/\Omega^2$ back into the original action (1) and obtain the low-energy effective action for the macroscopic electromagnetic field (in the laboratory frame):

$$\mathcal{L}_\mathrm{eff} = \frac{1}{2}\left[\left(1+\frac{g^2}{\Omega^2}\right)|\partial_t A|^2 - |\partial_x A|^2\right]. \tag{60}$$

As expected, the low-energy effective equation of motion from this action reproduces the dispersion relation (5). This action is analogous to that of a scalar field $A(t,x)$ in the effective metric

$$\mathrm{d}s_\mathrm{eff}^2 = \mathrm{d}t^2 - \left[1+\frac{g^2}{\Omega^2}\right]\left(\mathrm{d}x^2+\mathrm{d}y^2\right). \tag{61}$$

Note that an effective metric in 1+1 dimensions would not be sufficient (unless g/Ω is constant) because the effective action (60) is not conformally invariant. Furthermore, the above form is not unique—one could also use other choices (e.g., in 3+1 dimensions).

After a Lorentz boost to the pulse frame according to Eq. (6), the effective metric transforms to

$$\begin{aligned}\mathrm{d}s_\mathrm{eff}^2 = {}& \gamma^2\left(1-v^2\left[1+\frac{g^2}{\Omega^2}\right]\right)\mathrm{d}\tau^2 - 2v\gamma^2\frac{g^2}{\Omega^2}\,\mathrm{d}\tau\,\mathrm{d}\chi \\ & - \gamma^2\left(1+\frac{g^2}{\Omega^2}-v^2\right)\mathrm{d}\chi^2 \\ & - \left(1+\frac{g^2}{\Omega^2}\right)\mathrm{d}y^2 \ .\end{aligned} \tag{62}$$

Since $1/c_\mathrm{low}^2 = 1+g^2/\Omega^2$ according to Eq. (5), this corresponds to Eq. (26). Calculating the surface gravity from the above metric,

$$\kappa = \frac{1}{2}\left|\frac{\partial_\chi \mathfrak{g}_{00}^\mathrm{eff}}{\mathfrak{g}_{01}^\mathrm{eff}}\right|\Bigg|_\mathrm{horizon} = v\xi \ , \tag{63}$$

we find that the Hawking temperature is given by the standard expression (as expected)

$$T_\mathrm{H} = \frac{\kappa}{2\pi} = \frac{v\xi}{2\pi} \ . \tag{64}$$

Note that the transformation from the above stationary Painlevé–Gullstrand–Lemaître-type coordinates τ and χ to static Schwarzschild-type coordinates τ_* and χ via

$$\mathrm{d}\tau_* = \mathrm{d}\tau + \frac{\mathfrak{g}^{\mathrm{eff}}_{01}}{\mathfrak{g}^{\mathrm{eff}}_{00}}\,\mathrm{d}\chi \tag{65}$$

does not change the $\mathfrak{g}^{\mathrm{eff}}_{00}$ component of the metric,

$$\begin{aligned}\mathrm{d}s^2_{\mathrm{eff}} = {}& \gamma^2\left(1-v^2\left[1+\frac{g^2}{\Omega^2}\right]\right)\mathrm{d}\tau_*^2 \\ & - \gamma^{-2}\left(1-v^2\left[1+\frac{g^2}{\Omega^2}\right]\right)^{-1}\left(1+\frac{g^2}{\Omega^2}\right)\mathrm{d}\chi^2 \\ & - \left(1+\frac{g^2}{\Omega^2}\right)\mathrm{d}y^2\ .\end{aligned} \tag{66}$$

In complete analogy to the Schwarzschild metric, we may introduce the tortoise coordinate χ_* via

$$\mathrm{d}\chi_* = \gamma^{-2}\left(1-v^2\left[1+\frac{g^2}{\Omega^2}\right]\right)^{-1}\sqrt{1+\frac{g^2}{\Omega^2}}\,\mathrm{d}\chi\ , \tag{67}$$

such that the metric becomes

$$\begin{aligned}\mathrm{d}s^2_{\mathrm{eff}} = {}& \gamma^2\left(1-v^2\left[1+\frac{g^2}{\Omega^2}\right]\right)\left(\mathrm{d}\tau_*^2-\mathrm{d}\chi_*^2\right) \\ & - \left(1+\frac{g^2}{\Omega^2}\right)\mathrm{d}y^2\ .\end{aligned} \tag{68}$$

For a large $\chi_* \to +\infty$, this coordinate coincides with the original one, $\chi_* \approx \chi$, while the other limit, $\chi_* \to -\infty$, approaches the horizon, $\chi \downarrow 0$.

A. Breakdown of conformal invariance

The fact that the effective action (60) is not conformally invariant has important consequences. One of them is that left- and right-moving modes are not decoupled from each other. In our case, we find that the counterpropagating mode couples to the other modes (such as the Hawking radiation), which results in the second branch cut and the additional Bogoliubov coefficient η_ω, which in turn gives rise to the gray-body factor Γ_ω.

If we consider the limit where v approaches 1 (the vacuum speed of light), we find that g^2/Ω^2 becomes very small (near the horizon) and thus the effective action (60) is nearly conformal (even though one has to be careful with such an asymptotic statement). In this limit, the counterpropagating mode decouples approximately. Therefore, the second branch-cut contribution ($\psi^{\mathrm{cut}-}_\omega$) and the associated additional Bogoliubov coefficient η_ω go to zero such that the gray-body factor approaches unity and the Hawking temperature converges to the ordinary expression $\xi/(2\pi)$. As one can easily imagine, a pulse with a very small polarizability moving with almost the vacuum speed of light has very little impact on counterpropagating photons.

Note that the effective action (60) could be made conformally invariant if we added a magnetic permeability μ to the dielectric permittivity ε and demanded that $\varepsilon = \mu$. In this case, $\mathcal{L}_{\mathrm{eff}} = (\varepsilon|\partial_t A|^2 - |\partial_x A|^2/\mu)/2$, we may introduce an effective metric such as $\mathrm{d}s^2_{\mathrm{eff}} = \mathrm{d}t^2 - \varepsilon^2\mathrm{d}x^2$, which is 1+1 dimensional and thus can be cast into a conformally flat form. This conformal invariance leads to several simplifications (e.g., decoupling of left- and right-moving modes), which have been exploited in the literature; see, e.g., Refs. [5, 14, 17]. However—as we have seen above—these simplifications are not necessary for our purpose (the derivation of Hawking radiation). Of course, they can make not only obtaining but also interpreting the results easier. For example, as we discuss below in Sec. VIII, identifying the correct Hawking temperature in the case of broken conformal symmetry requires more care than in the conformally invariant situation, where one can easily read it off the Hawking spectrum.

B. Effective potential

The scattering of modes (coupling between left- and right-moving modes) due to the breakdown of conformal invariance can be understood nicely in terms of the effective potential. After transforming to the aforementioned tortoise coordinate χ_* and rescaling A_ω according to $\mathcal{A}_\omega = |\mathfrak{g}^{\mathrm{eff}}_{22}|^{1/4}A_\omega$, the wave equation reads

$$\left[\omega^2 + \frac{\partial^2}{\partial\chi_*^2} - V_{\mathrm{eff}}(\chi_*)\right]\mathcal{A}_\omega = 0\ , \tag{69}$$

with the effective potential

$$V_{\mathrm{eff}} = -v^2\xi^3\chi\,(1-v^2)\,\frac{2-(3+v^2)\xi\chi-16v^2\xi^2\chi^2}{(1+2\xi\chi)^3(1+2v^2\xi\chi)^3}\ . \tag{70}$$

For large $\chi_* \to +\infty$, this potential decreases as $1/\chi_*^3$ while in the other limit, $\chi_* \to -\infty$, it decreases exponentially (when approaching the horizon); see Fig. 7.

Note that Eq. (69) is formally equivalent to a Schrödinger scattering problem with the potential V_{eff} and the nonrelativistic energy $\mathcal{E} \propto \omega^2$. Thus, we get the usual transmission and reflection coefficients.

VIII. CONCLUSIONS

Based on the Hopfield model (1), we presented a fully relativistic derivation of the analog of Hawking radiation in a dispersive dielectric medium employing a minimal set of assumptions/approximations. As expected, we find that the Hawking temperature (55) is set by the surface gravity (63), but we also obtain a gray-body factor (56), which results in a nonthermal spectrum (54) observed at infinity.

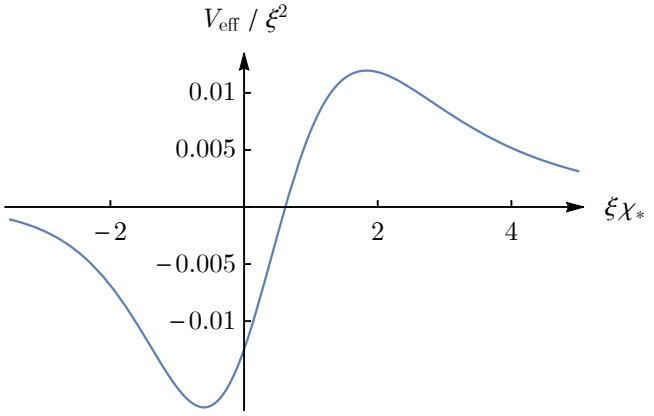

FIG. 7: Effective potential (70) outside the black hole as a function of the tortoise coordinate χ_* for $v = 2/3$ (however, the shape of the graph is generic for arbitrary pulse velocities). The coordinate transformation $\chi = \chi(\chi_*)$ was carried out numerically.

Let us emphasize that just this nonthermal spectrum $\langle\hat{\mathfrak{n}}^H_\omega\rangle_{\rm in} = |\beta_\omega|^2$ is not enough to determine the Hawking temperature. Instead, the Hawking temperature can be read off the ratio (53) of the Bogoliubov coefficients. This identification can be based on the following picture: imagine an initial short-wavelength wave packet composed of $k^+_\star$ and $k^-_\star$ modes with this ratio (53). Due to its short wavelength (and its thereby reduced group velocity), this wave packet approaches the horizon without scattering (by the effective potential $V_{\rm eff}$) and is constantly stretched during this approach (analog of gravitational redshift). Near the horizon, it is then stretched to long wavelengths and starts to escape to infinity as Hawking radiation (as its group velocity has increased). However, on the way out to infinity, part of this Hawking wave packet is scattered (by the effective potential $V_{\rm eff}$ due to the breaking of conformal invariance) and thereby transformed into a counterpropagating mode, which is then swallowed by the horizon. Now, in order to have only the Hawking mode at late times, we can send in an additional counterpropagating mode such that the two amplitudes (this direct counterpropagating mode and the scattered mode) beyond the horizon precisely cancel each other. This then leads to the form (48), which relates the final Hawking mode to a linear combination of initial short-wavelength modes (with amplitudes α_ω and β_ω) plus an initial counterpropagating mode (with the amplitude η_ω). In view of this scale separation (short and long wavelengths), we may distinguish the pure scattering process (leading to η_ω), which does not mix positive- and negative-norm states, from the mechanism of particle creation (involving the amplitudes α_ω and β_ω). The latter can be understood as an amplification process due to the horizon and is associated with the Hawking temperature, while the former gives rise to the gray-body factor.

As another way of demonstrating that the ratio (53) determines the Hawking temperature, let us reconstruct the analog of the Israel–Hartle–Hawking state (thermal equilibrium) and imagine sending in the long-wavelength modes in a thermal state with the temperature $T_{\rm in}$, while the short-wavelength modes are still in their vacuum state. In this situation, the expectation value for the Hawking particles reads

$$\begin{aligned}\langle\hat{\mathfrak{n}}^H_\omega\rangle_{\rm in} &= |\beta_\omega|^2 + |\eta_\omega|^2\,\langle\hat{\mathfrak{n}}^{\rm cp}_\omega\rangle_{\rm in}\\ &= \frac{1-|\eta_\omega|^2}{{\rm e}^{\omega/T_{\rm H}}-1} + \frac{|\eta_\omega|^2}{{\rm e}^{\omega/T_{\rm in}}-1}\,,\end{aligned} \tag{71}$$

where we have inserted the above result (54) for $|\beta_\omega|^2$ and the Bose–Einstein distribution (with temperature $T_{\rm in}$) for $\langle\hat{\mathfrak{n}}^{\rm cp}_\omega\rangle_{\rm in}$. We see that for $T_{\rm in} = T_{\rm H}$, we obtain a thermal spectrum for $\langle\hat{\mathfrak{n}}^H_\omega\rangle_{\rm in}$ with that temperature—which precisely corresponds to the detailed balance condition, as expected in a thermal equilibrium state.

Note that for obtaining the above results—such as the Hawking temperature as determined by the surface gravity and the gray-body factor—it is essential to take both branch cuts and thus also the counterpropagating mode into account. This might be one reason for the difference between our results and those in the recent paper [47]. In their paper, the second branch cut and the counterpropagating mode are apparently neglected and the Hawking temperature obtained there differs from our expression (and thus also from the surface gravity).

In our derivation, we had both branch cuts running upwards in the complex plane because this was most convenient for obtaining the solution which is evanescent inside the black hole; see the discussion of the boundary condition in Sec. IV B. For other choices of the branch cuts (with respect to the integration contour), we would obtain solutions with different boundary conditions. For example, having the two branch cuts run downwards to infinity (e.g., one in the bottom-right valley and the other one in the bottom-left valley), an analogous calculation would give the solution with the two initial short-wavelength solutions, $k^\pm_\star$, outside and the two final modes, $\tilde{k}^p_\star$ and $\tilde{k}^{\rm cp}_\star$, inside the black hole. In this way, by considering all possible combinations (both branch cuts up or both down or one up and one down), one can derive the 3×3 "scattering" matrix which connects the three initial modes, $k^\pm_\star$ and $k^{\rm cp}_\star$ (all outside), with the three final modes, $\tilde{k}^p_\star$ and $\tilde{k}^{\rm cp}_\star$ (inside), as well as $k^H_\star$ (outside).

ACKNOWLEDGMENTS

W.G.U. obtained support from Natural Sciences and Engineering Research Council of Canada (NSERC), the Templeton Foundation, and the Canadian Institute for Advanced Research. R.S. acknowledges support from Deutsche Forschungsgemeinschaft (SFB-TR12). We thank the Perimeter Institute for Theoretical Physics (PI), the Mainz Institute for Theoretical Physics (MITP), and the Pacific Institute of Theoretical Physics

(PITP), where part of this work was done, for their hospitality and support. R.S. also wishes to thank the Frankfurt Institute for Advanced Studies (FIAS) for the hospitality and support.

[1] S. W. Hawking, "Black hole explosions?" Nature **248**, 30–31 (1974).

[2] S. W. Hawking, "Particle creation by black holes," Commun. math. Phys. **43**, 199–220 (1975).

[3] W. G. Unruh, "Experimental Black-Hole Evaporation?" Phys. Rev. Lett. **46**, 1351–1353 (1981).

[4] W. G. Unruh, "Sonic analogue of black holes and the effects of high frequencies on black hole evaporation," Phys. Rev. D **51**, 2827–2838 (1995).

[5] R. Brout, S. Massar, R. Parentani, and Ph. Spindel, "Hawking radiation without trans-Planckian frequencies," Phys. Rev. D **52**, 4559–4568 (1995).

[6] T. Jacobson, "On the origin of the outgoing black hole modes," Phys. Rev. D **53**, 7082–7088 (1996).

[7] S. Corley and T. Jacobson, "Hawking spectrum and high frequency dispersion," Phys. Rev. D **54**, 1568–1586 (1996).

[8] M. Visser, "Acoustic black holes: horizons, ergospheres and Hawking radiation," Class. Quantum Grav. **15**, 1767–1791 (1998).

[9] S. Corley, "Computing the spectrum of black hole radiation in the presence of high frequency dispersion: An analytical approach," Phys. Rev. D **57**, 6280–6291 (1998).

[10] Y. Himemoto and T. Tanaka, "Generalization of the model of Hawking radiation with modified high frequency dispersion relation," Phys. Rev. D **61**, 064004 (2000).

[11] H. Saida and M. Sakagami, "Black hole radiation with high frequency dispersion," Phys. Rev. D **61**, 084023 (2000).

[12] W. G. Unruh and R. Schützhold, "Universality of the Hawking effect," Phys. Rev. D **71**, 024028 (2005).

[13] I. Agulló, J. Navarro-Salas, G. J. Olmo, and L. Parker, "Short-distance contribution to the spectrum of Hawking radiation," Phys. Rev. D **76**, 044018 (2007).

[14] R. Schützhold and W. G. Unruh, "Origin of the particles in black hole evaporation," Phys. Rev. D **78**, 041504 (2008).

[15] J. Macher and R. Parentani, "Black/white hole radiation from dispersive theories," Phys. Rev. D **79**, 124008 (2009).

[16] S. Finazzi and R. Parentani, "Spectral properties of acoustic black hole radiation: Broadening the horizon," Phys. Rev. D **83**, 084010 (2011).

[17] A. Coutant, R. Parentani, and S. Finazzi, "Black hole radiation with short distance dispersion, an analytical S-matrix approach," Phys. Rev. D **85**, 024021 (2012).

[18] S. Finazzi and R. Parentani, "Hawking radiation in dispersive theories, the two regimes," Phys. Rev. D **85**, 124027 (2012).

[19] A. Coutant and R. Parentani, "Hawking radiation with dispersion: The broadened horizon paradigm," Phys. Rev. D **90**, 121501 (2014).

[20] L. J. Garay, J. R. Anglin, J. I. Cirac, and P. Zoller, "Sonic analog of Gravitational Black Holes in Bose-Einstein Condensates," Phys. Rev. Lett. **85**, 4643–4647 (2000).

[21] L. J. Garay, J. R. Anglin, J. I. Cirac, and P. Zoller, "Sonic black holes in dilute Bose-Einstein condensates," Phys. Rev. A **63**, 023611 (2001).

[22] J. Macher and R. Parentani, "Black-hole radiation in Bose-Einstein condensates," Phys. Rev. A **80**, 043601 (2009).

[23] O. Lahav, A. Itah, A. Blumkin, C. Gordon, S. Rinott, A. Zayats, and J. Steinhauer, "Realization of a Sonic Black Hole Analog in a Bose-Einstein Condensate," Phys. Rev. Lett. **105**, 240401 (2010).

[24] J. Steinhauer, "Observation of self-amplifying Hawking radiation in an analogue black-hole laser," Nat. Phys. **10**, 864–869 (2014).

[25] T. A. Jacobson and G. E. Volovik, "Event horizons and ergoregions in ^{3}He," Phys. Rev. D **58**, 064021 (1998).

[26] U. Leonhardt and P. Piwnicki, "Optics of nonuniformly moving media," Phys. Rev. A **60**, 4301–4312 (1999).

[27] U. Leonhardt and P. Piwnicki, "Relativistic Effects of Light in Moving Media with Extremely Low Group Velocity," Phys. Rev. Lett. **84**, 822–825 (2000).

[28] M. Visser, "Comment on 'Relativistic Effects of Light in Moving Media with Extremely Low Group Velocity'," Phys. Rev. Lett. **85**, 5252 (2000).

[29] U. Leonhardt and P. Piwnicki, "Leonhardt and Piwnicki Reply:," Phys. Rev. Lett. **85**, 5253 (2000).

[30] W. G. Unruh and R. Schützhold, "On slow light as a black hole analogue," Phys. Rev. D **68**, 024008 (2003).

[31] R. Schützhold and W. G. Unruh, "Gravity wave analogues of black holes," Phys. Rev. D **66**, 044019 (2002).

[32] S. Giovanazzi, "Hawking Radiation in Sonic Black Holes," Phys. Rev. Lett. **94**, 061302 (2005).

[33] R. Schützhold and W. G. Unruh, "Hawking Radiation in an Electromagnetic Waveguide?" Phys. Rev. Lett. **95**, 031301 (2005).

[34] B. Horstmann, R. Schützhold, B. Reznik, S. Fagnocchi, and J. I. Cirac, "Hawking radiation on an ion ring in the quantum regime," New J. Phys. **13**, 045008 (2011).

[35] G. Rousseaux, C. Mathis, P. Maïssa, T. G. Philbin, and U. Leonhardt, "Observation of negative-frequency waves in a water tank: a classical analogue to the Hawking effect?" New J. Phys. **10**, 053015 (2008).

[36] S. Weinfurtner, E. W. Tedford, M. C. J. Penrice, W. G. Unruh, and G. A. Lawrence, "Measurement of Stimulated Hawking Emission in an Analogue System," Phys. Rev. Lett. **106**, 021302 (2011).

[37] R. Schützhold, G. Plunien, and G. Soff, "Dielectric Black Hole Analogs," Phys. Rev. Lett. **88**, 061101 (2002).

[38] T. G. Philbin, C. Kuklewicz, S. Robertson, S. Hill, F. König, and U. Leonhardt, "Fiber-Optical Analog of the Event Horizon," Science **319**, 1367–1370 (2008).

[39] D. Faccio, S. Cacciatori, V. Gorini, V. G. Sala, A. Averchi, A. Lotti, M. Kolesik, and J. V. Moloney, "Analogue gravity and ultrashort laser pulse filamentation," EPL **89**, 34004 (2010).

[40] F. Belgiorno, S. L. Cacciatori, G. Ortenzi, L. Rizzi, V. Gorini, and D. Faccio, "Dielectric black holes induced by a refractive index perturbation and the Hawking effect," Phys. Rev. D **83**, 024015 (2011).

[41] S. Finazzi and I. Carusotto, "Kinematic study of the

effect of dispersion in quantum vacuum emission from strong laser pulses," Eur. Phys. J. Plus **127**, 78 (2012).
[42] E. Rubino, A. Lotti, F. Belgiorno, S. L. Cacciatori, A. Couairon, U. Leonhardt, and D. Faccio, "Soliton-induced relativistic-scattering and amplification," Sci. Rep. **2**, 932 (2012).
[43] S. Finazzi and I. Carusotto, "Quantum vacuum emission in a nonlinear optical medium illuminated by a strong laser pulse," Phys. Rev. A **87**, 023803 (2013).
[44] M. Petev, N. Westerberg, D. Moss, E. Rubino, C. Rimoldi, S. L. Cacciatori, F. Belgiorno, and D. Faccio, "Blackbody Emission from Light Interacting with an Effective Moving Dispersive Medium," Phys. Rev. Lett. **111**, 043902 (2013).
[45] F. Belgiorno, S. L. Cacciatori, and F. Dalla Piazza, "Perturbative photon production in a dispersive medium," Eur. Phys. J. D **68**, 134 (2014).
[46] S. Finazzi and I. Carusotto, "Spontaneous quantum emission from analog white holes in a nonlinear optical medium," Phys. Rev. A **89**, 053807 (2014).
[47] F. Belgiorno, S. L. Cacciatori, and F. Dalla Piazza, "Hawking effect in dielectric media and the Hopfield model," Phys. Rev. D **91**, 124063 (2015).
[48] F. Belgiorno, S. L. Cacciatori, and F. Dalla Piazza, "The Hopfield model revisited: covariance and quantization," Phys. Scr. **91**, 015001 (2016).
[49] F. Belgiorno, S. L. Cacciatori, M. Clerici, V. Gorini, G. Ortenzi, L. Rizzi, E. Rubino, V. G. Sala, and D. Faccio, "Hawking Radiation from Ultrashort Laser Pulse Filaments," Phys. Rev. Lett. **105**, 203901 (2010).
[50] E. Rubino, F. Belgiorno, S. L. Cacciatori, M. Clerici, V. Gorini, G. Ortenzi, L. Rizzi, V. G. Sala, M. Kolesik, and D. Faccio, "Experimental evidence of analogue Hawking radiation from ultrashort laser pulse filaments," New J. Phys. **13**, 085005 (2011).
[51] R. Schützhold and W. G. Unruh, "Comment on 'Hawking Radiation from Ultrashort Laser Pulse Filaments'," Phys. Rev. Lett. **107**, 149401 (2011).
[52] F. Belgiorno, S. L. Cacciatori, M. Clerici, V. Gorini, G. Ortenzi, L. Rizzi, E. Rubino, V. G. Sala, and D. Faccio, "Belgiorno *et al.* Reply:," Phys. Rev. Lett. **107**, 149402 (2011).
[53] S. Liberati, A. Prain, and M. Visser, "Quantum vacuum radiation in optical glass," Phys. Rev. D **85**, 084014 (2012).
[54] W. G. Unruh and R. Schützhold, "Hawking radiation from 'phase horizons' in laser filaments?" Phys. Rev. D **86**, 064006 (2012).
[55] M. F. Linder, *Hawking radiation in dispersive dielectric media*, diploma thesis, Universität Duisburg-Essen (2013).
[56] J. J. Hopfield, "Theory of the Contribution of Excitons to the Complex Dielectric Constant of Crystals," Phys. Rev. **112**, 1555–1567 (1958).
[57] B. Huttner and S. M. Barnett, "Quantization of the electromagnetic field in dielectrics," Phys. Rev. A **46**, 4306–4322 (1992).
[58] D. Faccio, T. Arane, M. Lamperti, and U. Leonhardt, "Optical black hole lasers," Class. Quantum Grav. **29**, 224009 (2012).
[59] R. Schützhold and W. G. Unruh, "Hawking radiation with dispersion versus breakdown of the WKB approximation," Phys. Rev. D **88**, 124009 (2013).
[60] R. M. Wald, *General Relativity* (University of Chicago Press, Chicago, 1984).
[61] R. Wong, *Asymptotic Approximations of Integrals* (Society for Industrial and Applied Mathematics, Philadelphia, 2001).